LAWRENCE
LIVERMORE
NATIONAL
LABORATORY

LLNL-JRNL-609720

Evaluating adjusted forcing and model spread for historical and future scenarios in the CMIP5 generation of climate models

P. M. Forster, T. Andrews, P. Good, J. M. Gregory, L. S. Jackson, M. D. Zelinka

January 7, 2013

Journal of Geophysical Research - Atmospheres

Disclaimer

Evaluating adjusted forcing and model spread for historical and future scenarios in the CMIP5 generation of climate models

Piers M. Forster[(1)], Timothy Andrews[(2)], Peter Good[(2)], Jonathan M. Gregory[(2,3)], Lawrence S. Jackson[(1)], Mark Zelinka[(4)]

[1] School of Earth and Environment, University of Leeds, UK.

[2] Met Office Hadley Centre, Exeter, UK.

[3] NCAS-Climate, University of Reading, UK.

[4] PCMDI, Lawrence Livermore National Laboratory, U.S.

Corresponding Author: Piers Forster, School of Earth and Environment, University of Leeds, Leeds, LS2 9JT, UK. Email: p.m.forster@leeds.ac.uk

Abstract

We utilise energy budget diagnostics from the Coupled Model Intercomparison Project phase 5 (CMIP5) to evaluate the models' climate forcing since preindustrial times employing an established regression technique. The climate forcing evaluated this way, termed the adjusted forcing (AF), includes a rapid adjustment term associated with cloud changes and other tropospheric and land-surface changes. We estimate a 2010 total anthropogenic and natural AF from CMIP5 models of 1.9 ± 0.9 W m^{-2} (5-95% range). The projected AF of the Representative Concentration Pathway (RCP) simulations are lower than their expected radiative forcing (RF) in 2095 but agree well with efficacy weighted forcings from integrated assessment models. The smaller AF, compared to RF, is likely due to cloud adjustment. Multi-model time series of temperature change and AF from 1850 to 2100 have large inter-model spreads throughout the period. The inter-model spread of temperature change is principally driven by forcing differences in the present day and climate feedback differences in 2095, although forcing differences are still important for model spread at 2095. We find no significant relationship between the equilibrium climate sensitivity (ECS) of a model and its 2003 AF, in contrast to that found in older models where higher ECS models generally had less forcing. Given the large present day model spread there is no indication of any tendency by modelling groups to adjust their aerosol forcing in order to produce observed trends. Instead, some CMIP5 models have a relatively large positive forcing and overestimate the observed temperature change.

1. Introduction

Radiative forcings (RFs) are used extensively to quantify the drivers of climate change. Forcings can prove very useful in understanding differences between model responses to alternative forcing agents [*Shine and Forster*, 1999; *Hansen et al.*, 2005]. Offline comparisons between the radiative transfer codes used in atmosphere-ocean general circulation models (AOGCMs) with more accurate line-by-line codes have identified potentially important sources of error (> 20%) in how AOGCM radiative transfer codes compute radiative forcing [*Collins et al.*, 2006; *Forster et al.*, 2011] so it is important to test the veracity of their forcing estimates when running in coupled mode. However, this calculation of RF is difficult in practice and within climate models adjusted forcings (AFs) are more readily calculated from standard diagnostics using either fixed sea-surface temperature (SST) [*Hansen et al.*, 2005] or linear regression techniques [*Gregory et al.*, 2004].

Adjusted forcings are similar to RFs but additionally include rapid adjustments to the land-surface and troposphere that typically occur within a few days of applying a forcing and are largely due to cloud changes in the troposphere [*Andrews and Forster, 2008*; *Dong et al.*, 2009; *Andrews et al. 2012a*]. Importantly these rapid adjustments depend on the magnitude and nature of the forcing agent rather than on global mean temperature change [*Gregory and Webb*, 2008; *Andrews et al., 2010*], and it has been argued [*Rotstayn and Penner, 2001; Gregory and Forster, 2008; Lohmann et al., 2010; Bala et al., 2010*] that they are more appropriately regarded as forcings rather than feedbacks.

Forster and Taylor [2006], hereinafter FT06, developed a methodology to diagnose globally averaged AF in Coupled Model Intercomparison Project phase 3 (CMIP3) models and we use the same approach here within CMIP5 models, taking advantage of

their improved diagnostics and additional integrations to improve the methodology. We use these CMIP5 diagnostics to determine globally averaged AF components and energy budget changes since 1850 and use these to investigate how gross characteristics of the models evolve, concentrating on the factors influencing the spread of simulated time series for global average surface temperature and AF.

2. Methodology

The FT06 method makes use of a global linearized energy budget approach where the top of atmosphere (TOA) change in energy imbalance (N) is split between a climate forcing component (F) and a component associated with climate feedbacks that is proportional to globally averaged surface temperature change (ΔT), such that:

$$N = F - \alpha \Delta T \quad (1)$$

where α is the climate feedback parameter in units of W m^{-2} K^{-1}. To remove the effects of any preindustrial energy imbalance, N and ΔT are quantified as the difference from a preindustrial control simulation. CMIP5 models provide a long preindustrial control simulation from which the historical simulations branch. AOGCMs require a long spin up period for the ocean and their preindustrial control simulations are not necessarily in equilibrium. Further, even if the surface climate is near a steady state the TOA net radiation anomaly may still be non-zero as deep-ocean temperatures continue to evolve. The preindustrial climates of the CMIP5 models analysed were much closer to equilibrium and had less drift than the CMIP3 models. Nevertheless, some energy imbalance remained (Figure 1). In most models this imbalance was due to problems with closure of their energy budgets rather than a discernible drift. To address this, the individual flux terms and temperatures used in equation 1 were generated by subtracting any imbalance and its

drift from the equivalent segment of each model's own preindustrial control simulation. This drift was calculated as a linear trend over the control segment and removed from the N and ΔT timeseries of the forced scenarios.

AS in FT06 we use a two step process to derive timeseries for F. Step 1 uses CO_2-only climate-simulations to diagnose α terms using linear regression. As in Andrews et al. [*2012b*] this analysis uses the CMIP5 abrupt $4xCO_2$ simulations and regresses N against ΔT to diagnose the $4xCO_2$ AF as an intercept term and α as the slope of the regression line. Component α terms are presented in Table 1. Then, assuming α is both independent of forcing agent and time invariant, Step 2 employs equation 1 to diagnose the timeseries for F in a transient scenario run, using diagnostics of N and ΔT. In step 2 we substitute these α terms into equation 1, using N and ΔT diagnostics from various forced scenarios to compute each model's AF. The AF calculation is performed for the three historical scenarios from the late 19th century to 2005 (*Historical* - all natural and anthropogenic forcings; *HistoricalGHG* - long-lived greenhouse gas changes only; and *HistoricalNat* - natural solar and volcanic forcings only), and the four Representative Concentration Pathways of future anthropogenic changes in atmospheric composition (RCP2.6, RCP4.5, RCP6.0 and RCP8.5). These RCPs are named after the 2100 radiative forcing they aim to generate relative to 1750 [*Meinshausen et al.*, 2011]. RCP2.6 should have a peak radiative forcing of 3 W m^{-2} declining to 2.6 W m^{-2} by 2100. RCP4.5 and RCP 6.0 should have radiative forcings close to 4.5 W m^{-2} and 6.0 W m^{-2}, respectively, on stabilisation of greenhouse gas concentrations after 2100. RCP8.5 should lead to a radiative forcing close to 8.5 W m^{-2} by 2100. However, Meinshausen et al. [2011] found that integrated

assessment models generated smaller RFs in 2100, namely 2.5, 4.1, 5.3 and 8.2 W m^{-2} for RCP2.6, RCP4.5, RCP6.0 and RCP8.5 respectively.

The original FT06 analysis differed from the analysis here (hereinafter referred to as FT06-updated) into its approach to step 1. In the original FT06 method, each modeling groups' estimate of their model's 2xCO_2 radiative forcing, along with N and ΔT values from 1% per year CO_2 increase runs, were used to determine α. The radiative forcing was taken as the stratospherically adjusted Intergovernmental Panel on Climate Change (IPCC) forcing definition [*Ramaswamy et al.*, 2001], whereas the forcing methodology in Step 2 has a component of rapid adjustment, as the N timeseries used to diagnose F was measured as monthly TOA fluxes in a scenario integration that would be continually adjusting to the underlying forcing. Therefore steps 1 and 2 in the original method used inconsistent forcing definitions. By contrast, in FT06-updated, step 1 diagnoses both AF and α as the intercept and slope of the regression line respectively, and therefore uses AF consistently in steps 1 and 2.

To elucidate the role of historical forcings other than greenhouse gases, the *HistoricalNat* and *HistoricalGHG* scenarios were subtracted from the full historical simulation. Assuming linearity, the resulting residual *Historical-nonGHG* scenario was taken to represent the combined effects of aerosol as well as any land-use and ozone changes. Previous assessments have suggested that forcings from ozone and land-use could more or less cancel each other in the global mean so that this residual would dominated by aerosol effects [*Forster et al.*, 2007; *Skeie et al.*, 2011]. For example, *Forster et al.* [2007] estimated global mean RFs in 2005 of: +0.3 W m^{-2} from ozone changes; -0.2 W m^{-2} from

133 land-use albedo changes; and -0.5 W m^{-2} and -0.7 W m^{-2} for aerosol direct and indirect
134 effects respectively.

135 Not all models had the complete set of energy budget variables needed for the sensitivity
136 and forcing analysis. The models in Table 1 were those with the necessary data, as of
137 November 2012. All available ensemble members were used in the analysis and averaged
138 over.

139 **3. Adjusted Forcings**

140 Figure 2 shows the time evolution of globally averaged surface temperature and calculated
141 AF, relative to the preindustrial climate, for historical and future scenarios. The variation
142 of AF across models and scenarios is shown in Figure 3. Figure 4 breaks down the
143 components of AF in the models for year 2003 (2001-2005 average) and year 2095 (2090-
144 2100 average).

145 AFs for the individual models in these years are given in Table 2. In the historical
146 simulations, the 2003 AF (2001-2005 average) was found to be 1.7 ± 0.9 W m^{-2} from the
147 *Historical* simulation, 2.4 ± 0.8 W m^{-2} from the *HistoricalGHG* simulation, 0.1 ± 0.2 W
148 m^{-2} from the *HistoricalNat* simulation, and -0.8 ± 0.9 W m^{-2} from the *Historical-nonGHG*
149 residual simulation. This gives an anthropogenic (*Historical* minus *HistoricalNat*) AF of
150 1.6 W m^{-2} ± 0.8 in 2003. All errors represent the 5%-95% model range. Multi-model mean
151 AFs for the RCP scenarios all depart from their expected radiative forcings (Table 2 and
152 Figure 2). RCP forcing estimates in 2095 are less than their targeted forcing, but agree
153 very well with the forcing estimates derived from Integrated Assessment Modelling
154 [*Mienshausen et al., 2011*]. When the different efficacies of the various forcing agents are
155 accounted for, *Mienshausen et al.* finds effective forcings in 2095 of 2.3, 3.9, 5.2 and 8.0

156 Wm^{-2} for RCP2.6, RCP4.5, RCP6.0 and RCP8.5 respectively, within 10% of the CMIP5
157 model-mean given in Table 2.

158 The 5% to 95% uncertainty range of AF in the *HistoricalGHG* simulation in 2003 is ± 0.8
159 W m^{-2}, which is nearly as large as the spread associated with non greenhouse gas AF
160 (Table 2). The evolution of net AF and surface temperature shows considerable spread
161 among models (Figures 2 and 3). The fractional spread of net AF tends to grow much
162 more in the historical period than in the future (Figure 3). Examining Figure 3a and Table
163 2, natural forcing differences contribute least to the fractional model spread and
164 greenhouse gas and non greenhouse gas forcing contribute in roughly equal proportions.

165 Figure 4 examines the components of AF. The positive longwave (LW) clear-sky forcing
166 is associated with greenhouse gas changes and has least spread between models. The
167 cloud AF terms are calculated from anomalies in cloud radiative effect (CRE) where all-
168 sky and clear sky fluxes are differenced. Because radiative anomalies due to changes in
169 forcing agents, water vapor, surface albedo, etc. are smaller in the presence of clouds than
170 they would be in the absence of clouds, CRE-derived cloud AF estimates include a
171 component of cloud masking. Model differences in aerosol forcings, rapid adjustments
172 and/or cloud masking effects can all contribute to the CRE-derived cloud AF spread.
173 [*Zelinka et al., manuscript in revision, 2012*]. A LW cloud masking effect of roughly +0.6
174 W m^{-2} is expected from a doubling of CO_2 [*Andrews and Forster*, 2008; *Soden et al.*,
175 2008; *Colman and McAvaney*, 2011]. We adopt the sign convention that the cloud
176 masking effect represents an additional positive forcing that needs to be added to CRE-
177 derived terms. As the forcing from CO_2 is currently around half of its doubled CO_2 value,
178 this suggests that around +0.3 W m^{-2} of cloud masking needs to be added to the *Historical*
179 CRE-derived cloud AF terms. The RCP 8.5 CRE-derived cloud AF would need to have a

larger component of masking added, around +0.6 W m^{-2}. The shortwave (SW) clear-sky AF and CRE-derived cloud AF split would also be affected by cloud masking of sea-ice changes. Nevertheless, a negative CRE-derived cloud AF beyond that which is expected from cloud masking is seen in all the scenarios in Figure 4.

The *Historical-nonGHG* AF shows a generally negative trend that turned weakly positive around 1990 in most models (Figures 2 and 3), although some models show a strongly negative AF and others have an AF near zero or slightly positive (Figure 3). Because of the multiple forcing agents represented in the *Historical-nonGHG* scenario, the CMIP5 model spread in its AF of -0.8 ± 0.9 W m^{-2} in 2003 is difficult to interpret (see Section 4).

4. Comparing forcing definitions

In order to interpret the AFs given in Section 3 it is important to understand their uncertainty. Here we test three aspects of the analysis: i) limitations of the two step AF process; ii) representing cloud AF using CRE-derived AFs; iii) using the *Historical-nonGHG* scenario as a proxy for aerosol AF.

i) Limitations of the two step AF process

FT06 found that forcings from the 2-step regression procedure agreed with offline radiative forcing calculations in two models. However, variation in climate sensitivity could in principle bias the AF estimates. While some bias cannot be ruled out, for a scenario with CO_2 increasing at 1% per year, ensemble mean AF (derived using the FT06-updated method) has been found to increase linearly with time (to within the precision set by internal variability), as expected if climate sensitivity were approximately constant [*Good et al. 2012*]. To test this further, we compared the FT06-updated AF with an AF

derived from transient experiments where SSTs are prescribed from observations [*Held et al.*, 2010]. The SST-derived method used two transient integrations, one with forcing agents and one without. The run with changes in forcing agents gives a heat balance described by equation 1 and the run without changes in forcing agents gives a heat balance described by (note the primes):

$$N' = F' - \alpha \Delta T' \quad (2)$$

where F' = 0 by definition. As SSTs are identically prescribed in both, $\Delta T \sim \Delta T'$, and substituting (2) into (1) gives:

$$F = N - N' \quad (3)$$

AFs derived from these two definitions are compared in Figure 5. Although there is considerable variability in the FT06-updated AF, its AF seems to agree very well with the prescribed SST-derived AF from a 10-ensemble member average in this one CMIP3 model. The AFs calculated from the two methods could diverge if the integration continued beyond 2000 out to 2100. Nevertheless, this comparison gives some confidence that differences between the FT06-updated AF and other AF estimates are comparable and not affected by an error associated with possible climate sensitivity drift with the FT06-updated methodology.

ii) Representing cloud AF using CRE-derived AFs

To test the CRE-derived AF estimates and examine if they arise from a rapid adjustment of cloud or from cloud masking, cloud-induced radiation anomalies can be computed directly from cloud anomalies diagnosed by the ISCCP simulator [*Klein and Jakob 1999;*

Webb et al. 2001] in combination with cloud radiative kernels [*Zelinka et al. 2012*]. The kernels quantify the impact on TOA radiative fluxes of cloud fraction perturbations for each of the 49 different ISCCP simulator cloud types. Multiplying cloud fraction anomalies by the kernels yields TOA radiation anomalies that are purely a result of cloud changes and are free of any non-cloud effects. Therefore we refer to the cloud AFs and feedbacks that are computed from these cloud-induced anomalies as "unmasked," to be distinguished from those derived using CRE, which include masking effects.

To derive cloud AFs, we follow the exact same FT06-updated procedure as described in Section 2, but replace N in equation 1 with cloud-induced radiative flux anomalies, so that α is the unmasked cloud feedback. The unmasked cloud feedback α terms are derived from the abrupt $4xCO_2$ runs in Zelinka et al., (manuscript under revision 2012) for the five models that have archived the necessary diagnostics. The CRE-derived and unmasked LW, SW, and net cloud AFs in 2003 for the *Historical* run are compared in Figure 6. As expected, the unmasked LW cloud AF is systematically more positive than the CRE-derived value in every model (0.56 W m^{-2} larger on average) and the unmasked SW cloud AF is systematically less positive or more negative than the CRE-derived value (0.32 W m^{-2} smaller on average). This brings the unmasked negative net cloud AF in 2003 closer to zero (-0.33 rather than -0.57 W m^{-2}) and increases the spread in this quantity among the five models. That the unmasked net cloud AF is non-zero indicates that cloud rapid adjustments are physically occurring, and are tending to reduce the effective climate forcing. The difference between the unmasked and CRE-derived cloud AFs quantifies the amount of cloud masking in the Section 3 estimates of AF. The net cloud masking effect at the end of the *Historical* run in these 5 models is systematically positive and averages to

0.24 W m^{-2}. In agreement with expectations from Section 3, this is roughly half of the value expected for doubling of CO_2.

The SW cloud AF dominates over the LW cloud AF in every model, in agreement with previous studies. However, *Zelinka et al.* [*manuscript under revision, 2012*] find a positive unmasked SW rapid adjustment cloud AF under 4xCO_2 for all 5 models, which raises the question of why most (3 out of these 5) models give negative unmasked SW cloud AFs in 2003 given that CO_2 is the dominant forcing agent in the latter part of the *Historical* run. This may be evidence that the non-CO_2 forcing agents (which are present in the *Historical* run but not in the idealized 4xCO_2 runs) cause significant cloud adjustments, even if they are not the ones responsible for most of the unadjusted forcing (just like cloud feedbacks are responsible for most of the spread in climate feedback, whereas water vapor is responsible for most of the ensemble mean feedback). Previous studies have found large cloud forcing from rapid adjustments associated with perturbations to the solar constant, black carbon, and ozone [*e.g. Hansen et al., 2005; Bala et al. 2010; Ban Weiss et al. 2011*] but these cloud forcing vary considerably between the location and magnitude of the forcing agent and the model. On the other hand our diagnosed cloud AF could be an artefact of the assumptions inherent in the 2-step regression technique.

iii) Using the *Historical-nonGHG* scenario as a proxy for aerosol AF.

To test the aerosol AF estimate, we examined fixed SST experiments existing in the CMIP5 archive. In these experiments individual forcing agents have been introduced; present day aerosol perturbation experiments exist for three models and their AFs can be compared to the FT06-updated AFs, taken from the *Historical-nonGHG* simulations. The

fixed-SST AFs are taken as the difference of TOA fluxes between a forced and a preindustrial control experiment (as in equation 3). These AFs are given in Table 4, which also shows AFs from the FT06-updated method, repeated from Table 2. The AFs derived by the two methods are appreciably different, indicating that other non-greenhouse forcing agents, such as land-use and ozone, as well as the aerosol signal affect the *Historical-nonGHG* simulations.

This section has shown that it is not appropriate to represent aerosol AF by the *Historical-nonGHG* residual scenario and that CRE-derived cloud AFs may not be representative of actual AFs from rapid cloud adjustment. Nevertheless the *net* AF does correctly capture both radiative forcing and cloud adjustment and could be expected to match other AF estimates over 1850-2100 simulations and can therefore provide useful insights into the causes of global-mean temperature change, examined next.

5. Inter-model temperature spread

This section uses the AFs diagnosed in Section 3 to help understand the gross characteristics of the CMIP5 models' surface temperature response. In particular, we focus on how differences in forcing and climate sensitivity affect the inter-model spread of surface temperature change.

A model's historical temperature trend depends on forcing, climate sensitivity and ocean heat uptake. As aerosol forcing and climate sensitivity are uncertain, modeling centers could be modifying their controlling factors to reproduce the observed globally averaged 20th century temperature trends as well as possible. There was some evidence of a trade off between climate sensitivity and forcing in CMIP3 and earlier generations of models [*Kiehl*, 2007; *Knutti*, 2008]. Figure 7 reproduces Figure 1 of *Kiehl* [2007] for CMIP5

models and finds considerably smaller correlation than in either the CMIP3 analysis of *Knutti* [2008] or the older model analysis of *Kiehl* [2007] that are reproduced as blue and red symbols respectively. The R^2 fit in CMIP5 models is slightly smaller than in CMIP3 models and is not significant. The green squares show a subset of the CMIP5 models that match the observed century-scale linear temperature trends (0.57 to 0.92 K increase over 1906-2006, *IPCC* [2007]). This subset reproduces the *Kiehl* [2007] fit almost perfectly. The CMIP5 models that are not in this grouping tend to have a larger positive AF compared to those that match observations and thereby overestimate the observed temperature trend. Variation in the magnitude of the CO_2 AF affects both the AF in 2003 and the ECS. Figure 8 shows that both AF in 2003 and the $2xCO_2$ AF are positively correlated with α [see also *Andrews et al., 2012b*]. This means that models with smaller sensitivities tend to also have smaller CO_2 AFs which would act to converge models towards similar *Historical* temperature responses.

The transient response of a model depends on ocean heat uptake as well as the Equilibrium Climate Sensitivity (ECS). If modelling groups are adjusting forcing to match the observed temperature trends then one might expect that the correlation between 2003 AF and the transient climate response (TCR) to be larger than the correlation between 2003 AF and ECS. However, these correlations are -0.11 and -0.41 respectively and neither is significant at the 5% level.

The causes of model spread can be further examined by using the approach of *Gregory and Forster* [2008], whereby the global mean temperature change under a scenario of continually increasing forcing is:

317 $$\Delta T = F / \rho \quad (4)$$

318 where the climate resistance $\rho = \alpha + \kappa$, κ being the ocean heat uptake efficiency.

319 The estimates of ρ and κ from the 1% per year CO_2 increase simulations are given in
320 Table 1. The α values used are derived from the $4xCO_2$ abrupt integration from Section 3
321 and are also presented in Table 1. The α values derived from the 1% per year CO_2
322 increase integration (not shown) were very similar to values diagnosed from the $4xCO_2$
323 abrupt integration [*see also Kuhlbrodt and Gregory, 2012*]. Figure 9 examines how AF in
324 2003, ρ, α, κ influence the temperature change. As expected, AF / ρ (Figure 9a) explains
325 most of the variation in temperature, and AF (Figure 9b) is by far the most important
326 influence. Models with a *Historical* AF in 2003 that is more positive than about 2 Wm^{-2}
327 typically have a temperature change that is larger than observed. In contrast, ρ, α and κ
328 (Figures 9c,d and e) show no systematic tendency for affecting temperature. For example
329 the HadGEM2-ES and GFDL-CM3 models exhibit two of the smallest temperature
330 changes but also have two of the smallest α values (high ECS). Therefore their small
331 temperature change results primarily from a small forcing. These results suggest that AF
332 in some models may be too positive to accurately reproduce historic temperature trends.

333 Multiple linear regression was used to model the CMIP5 spread of temperatures using
334 explanatory variables of AF, α, ρ, and κ from Tables 1 and 2. Of these, the strongest
335 correlation was found between AF and α at 0.62 (see Figure 8a). ρ and κ were somewhat
336 positively correlated with F, but not by as much (0.45 and 0.02 respectively). These
337 correlations mean that whilst models with larger AF generally have larger feedback
338 parameters (smaller sensitivities) and more efficient ocean heat uptake (larger κ), no clear
339 pattern of compensation emerges between climate model feedback parameters, or ocean
340 heat uptake, and AF (see also Figure 9).

Figure 10 compares ρ derived from two RCPs with increasing forcing over 2000-2050, with ρ derived from the 1% per year CO_2 increase simulation that is used to define TCR. Estimates of ρ are generally well correlated between the RCP scenarios and the 1% per year CO_2 increase simulation. κ values are not shown but follow a similar pattern. The 1% per year run has a larger forcing increase than RCP 8.5 and models have a consistently larger κ and ρ for this scenario than those derived from the other scenarios. Likewise, RCP8.5, compared to RCP 4.5 has a larger forcing increase and larger κ and ρ over the period. A more rapid forcing increase would be better at maintaining stronger vertical temperature gradients within the ocean. These would be expected to be more efficient at transferring heat from the surface to the subsurface ocean, leading to a larger κ and, therefore, a larger ρ value.

Figure 11a shows how the standard deviation in AF and temperature change projections between models varies with time for the RCP 8.5 scenario. Note the similarity of the two quantities, consistent with the expectation from equation 4 that temperature change is proportional to AF if climate resistance is constant. The coefficient of variation (standard deviation/mean) is largest for the present day (Figure 11b) because the standard deviation does not grow as rapidly as the model-mean.

Examining model spread, an across-model regression of temperature change simultaneously against α and AF gave a good fit to the data for both 2010 and 2095 (see Figure 12). In RCP4.5 this regression explained 72% of the variation in temperature change and slope coefficients for both AF and α were statistically significant at the 0.1% significance level. For 2010 data, AF explained the largest proportion of variation in the temperature change (49%) with α improving the fit across the full range of temperature

365 changes. In contrast, α explained the largest proportion of variation in the temperature
366 change in the 2095 data (42%) with forcing improving the fit particularly for data points
367 with more extreme (both large and small) temperature changes. Temperature change is
368 much more sensitive to variations in α in the 2095 data than in the 2010 data, with a
369 regression slope coefficient of 1.45 ± 0.22 for 2095 compared to 0.56 ± 0.21 for 2010.
370 There was no significant difference in sensitivity to AF between 2010 and 2095.

371 This analysis shows that large forcing differences between models today give a large
372 spread in model temperature change. This is likely due to the current strong aerosol
373 forcing that varies considerably between models, but this aerosol forcing is projected to
374 weaken. Any relationship between α and AF has little effect on model spread and there is
375 no indication of models herding towards similar 20th century temperature trends. In the
376 future the role of forcing remains important and, therefore, differences in forcing will need
377 to be considered when comparing model simulations within a given scenario.

378 **6. Discussion and Conclusions**

379 The estimated anthropogenic AF of 1.6 W m^{-2} ± 0.9 and the estimated greenhouse gas AF
380 of 2.4 ± 0.8 W m^{-2} in 2003 agree well with the last IPCC report and more recent estimates
381 of radiative forcing, even though the definition of the two forcings differ. For example
382 *Forster et al.* [2007] estimated a total anthropogenic forcing of 1.6 ± 1.0 W m^{-2} in 2005
383 and *Skeie et al.* [2011] estimated a year 2000 greenhouse gas RF of 2.5 W m^{-2}.

384 The total AF from CMIP5 models, estimated to be 1.7 ± 0.9 W m^{-2} in 2003, grows to 1.9 ±
385 0.9 Wm^{-2} in 2010. In contrast to the IPCC estimate, where the spread was principally
386 attributed to aerosols, the spread found here comes from both non-greenhouse gas forcing
387 agents and differences in the rapid adjustment of cloud to greenhouse gases.

The AF estimates made in this paper include a significant cloud component that acts to make the AF smaller than the expected RF. Because of this, the projected 2095 AFs are lower than the corresponding estimate of RF from the original RCP scenario. However, they agree well with the effective forcing estimate of the integrated assessment models [*Meinshausen et al.*, 2011]. Consistent with a lower AF, *Andrews et al.* [2012b] found that CMIP5 models had a 4xCO_2 AF that ranged between 5.6 and 8.5 W m^{-2}, and was, on average, 0.4 W m^{-2} lower than the expected RF of 7.4 W m^{-2}. Figures 1 and 3 in *Andrews et al.* [2012b] suggest that rapid adjustments within this framework are not necessarily an immediate physical cloud change but could also be associated, in some AOGCMs, with a non-linear response in SW CRE principally found over oceans. This is further supported in Zelinka et al. (manuscript in preparation, 2012) who show that unmasked cloud AFs diagnosed using this linear framework (i.e. the linear regression line intercept) tend to be negatively biased with respect to those diagnosed in fixed SST and perturbed CO_2 simulations. These caveats limit our ability to interpret RF and AF differences as a genuine cloud adjustment.

Generally it would be useful to test the FT06-updated approach under a wider set of models and scenarios to better quantify and understand its errors, quantify differences with other AF methodologies, and quantify the role of rapid adjustment.

Issues remain around the definitions of AF and the assumption of constant climate sensitivity within a transient forcing framework. The forcing/climate sensitivity concept developed essentially for slab-ocean models at equilibrium obviously does not provide a complete picture of climate evolution in today's non-linear AOGCMs. Nevertheless, we argue that forcings are useful for understanding why models differ in their gross behaviour and forcings explain the spread of RCP projections rather well. Careful analysis of the

412 Earth’s energy budget examining climate response on multiple timescales is
413 recommended.

414 **Acknowledgements**

415 PF was supported by EPSRC grant EP/I014721/1 and A Royal Society Wolfson Merit
416 Award. We acknowledge the World Climate Research Programme's Working Group on
417 Coupled Modelling, which is responsible for CMIP, and we thank the climate modelling
418 groups (listed in Table 1 of this paper) for producing and making available their model
419 output. For CMIP the U.S. Department of Energy's Program for Climate Model Diagnosis
420 and Intercomparison provides coordinating support and led development of software
421 infrastructure in partnership with the Global Organization for Earth System Science
422 Portals. TA and JG were supported by the Joint DECC/Defra Met Office Hadley Centre
423 Climate Programme (GA01101). We thank Isaac Held for providing the forcing data from
424 Held et al. [*2010*]. The contribution of MDZ was performed under the auspices of U.S.
425 Department of Energy by Lawrence Livermore National Laboratory (LLNL) under
426 Contract DE-AC52-07NA27344 and was supported by the LLNL Institutional
427 Postdoctoral Program. Very helpful review comments were provided by Jeff Kiehl, Jean-
428 Louis Defresne and an anonymous referee.

429 **References**

430 Andrews, T., and P. M. Forster (2008), CO_2 forcing induces semi-direct effects with
431 consequences for climate feedback interpretations, *Geophysical Research Letters, 35*,
432 L04802.

433 Andrews, T., P. M. Forster, O. Boucher, N. Bellouin, and A. Jones (2010), Precipitation,
434 radiative forcing and global temperature change, *Geophysical Research Letters, 37*,
435 L14701.

436 Andrews, T., J.M. Gregory, P.M. Forster and M.J. Webb (2012a) Cloud adjustment and
437 its role in CO2 radiative forcing and climate sensitivity: A review. Surveys in Geophysics,
438 33, 619-635, doi:10.1007/s10712-011-9152-0.)

439 Andrews, T., J. M. Gregory, M. J. Webb, and K. E. Taylor (2012b), Forcing, feedbacks
440 and climate sensitivity in CMIP5 coupled atmosphere-ocean climate models, *Geophysical*
441 *Research Letters*, *39*, L09712.

442 Ban-Weiss, George A., L. Cao, G. Bala, K. Caldeira (2011), Dependence of climate
443 forcing and response on the altitude of black carbon aerosols, *Climate Dynamics*, DOI:
444 10.1007/s00382-011-1052-y

445 Bala, G., K. Caldeira, and R. Nemani (2009), Fast versus slow response in climate change:
446 implications for the global hydrological cycle, *Climate Dynamics*, *35*, 423-434.

447 Church, J. A., N. J. White, L. F. Konikow, C. M. Domingues, J. G. Cogley, E. Rignot, J.
448 M. Gregory, M. R. van den Broeke, A. J. Monaghan, and I. Velicogna (2011), Revisiting
449 the Earth's sea-level and energy budgets from 1961 to 2008, *Geophysical Research*
450 *Letters*, *38*, L18601.

Collins, W. D., V. Ramaswamy, M. D. Schwarzkopf, Y. Sun, R. W. Portmann, Q. Fu, S. E. B. Casanova, J.-L. Dufresne, D. W. Fillmore, P. M. D. Forster, V. Y. Galin, L. K. Gohar, W. J. Ingram, D. P. Kratz, M.-P. Lefebvre, J. Li, P. Marquet, V. Oinas, Y. Tsushiman, T. Uchiyama, and W. Y. Zhong (2006), Radiative forcing by well-mixed greenhouse gases: Estimates from climate models in the Intergovernmental Panel on Climate Change (IPCC) Fourth Assessment Report (AR4), *Journal of Geophysical Research-Atmospheres*, *111*, D14317.

Colman, R. A., and B. J. McAvaney (2011), On tropospheric adjustment to forcing and climate feedbacks, *Climate Dynamics*, *36*(9-10), 1649-1658.

Dong, B. W., J. M. Gregory, and R. T. Sutton (2009), Understanding Land-Sea Warming Contrast in Response to Increasing Greenhouse Gases. Part I: Transient Adjustment, *Journal of Climate*, *22*(11), 3079-3097.

Forster, P. M., and K. Taylor (2006), Climate forcings and climate sensitivities diagnosed from coupled climate model integrations, *Journal of Climate*, 6181-6194.

Forster, P., V. Ramaswamy, P. Artaxo, T. Berntsen, R. Betts, D.W. Fahey, J. Haywood, J. Lean, D.C. Lowe, G. Myhre, J. Nganga, R. Prinn, G. Raga, M. Schulz and R. Van Dorland, 2007: Changes in Atmospheric Constituents and in Radiative Forcing. In: Climate Change 2007: The Physical Science Basis. Contribution of Working Group I to the Fourth Assessment Report of the Intergovernmental Panel on Climate Change [Solomon, S., D. Qin, M. Manning, Z. Chen, M. Marquis, K.B. Averyt, M.Tignor, and H.L. Miller (eds.)]. Cambridge University Press, Cambridge, United Kingdom and New York, NY, USA.

Forster, P. M., V. I. Fomichev, E. Rozanov, C. Cagnazzo, A. I. Jonsson, U. Langematz, B. Fomin, M. J. Iacono, B. Mayer, E. Mlawer, G. Myhre, R. W. Portmann, H. Akiyoshi, V. Falaleeva, N. Gillett, A. Karpechko, J. Li, P. Lemennais, O. Morgenstern, S. Oberländer, M. Sigmond, and K. Shibata (2011), Evaluation of radiation scheme performance within chemistry climate models, *Journal of Geophysical Research-Atmospheres*, *116*.

Good, P., J. M. Gregory, J. Lowe, and T. Andrews (2012), Abrupt CO_2 experiments as tools for predicting and understanding CMIP5 representative concentration pathway projections, *Climate Dynamics*, DOI: 10.1007/s00382-012-1410-4.

Gregory, J. M., W. Ingram, M. Palmer, G. Jones, P. Stott, R. Thorpe, J. Lowe, T. Johns, and K. Williams (2004), A new method for diagnosing radiative forcing and climate sensitivity, *Geophysical Research Letters*, *31*, L03205.

Gregory, J. M., and P. Forster (2008), Transient climate response estimated from radiative forcing and observed temperature change, *Journal of Geophysical Research-Atmospheres*, *113*, D23105.

Gregory, J. M., and M. Webb (2008), Tropospheric adjustment induces a cloud component in CO_2 forcing, *Journal of Climate*, *21*(1), 58-71.

Hansen, J., M. Sato, R. Ruedy, L. Nazarenko, A. Lacis, G.A. Schmidt, G. Russell, I. Aleinov, M. Bauer, S. Bauer, N. Bell, B. Cairns, V. Canuto, M. Chandler, Y. Cheng, A. Del Genio, G. Faluvegi, E. Fleming, A. Friend, T. Hall, C. Jackman, M. Kelley, N.Y. Kiang, D. Koch, J. Lean, J. Lerner, K. Lo, S. Menon, R.L. Miller, P. Minnis, T. Novakov, V. Oinas, J.P. Perlwitz, Ju. Perlwitz, D. Rind, A. Romanou, D. Shindell, P. Stone, S. Sun, N. Tausnev, D. Thresher, B. Wielicki, T. Wong, M. Yao, and S. Zhang, (2005), Efficacy

495 of climate forcings, *Journal of Geophysical Research*, *110*, D18104,
496 doi:10.1029/2005JD005776.

497 Hansen, J., M. Sato, P. Kharecha, and K. von Schuckmann (2011), Earth's energy
498 imbalance and implications, *Atmospheric Chemistry and Physics*, *11*, 13421-13449.

499 Held, I., M. Winton, K. Takahashi, T. Delworth, F. Zeng, and G. Vallis (2010), Probing
500 the Fast and Slow Components of Global Warming by Returning Abruptly to Preindustrial
501 Forcing, *Journal of Climate*, *23*(9), 2418-2427.

502 Kiehl, J. T. (2007), Twentieth century climate model response and climate sensitivity,
503 *Geophysical Research Letters*, *34*, L22710.

504 Klein, S. A., and C. Jakob (1999), Validation and sensitivities of frontal clouds simulated
505 by the ECMWF model, *Mon. Weather Rev.*, *127*, 2514–2531.

506 Knutti, R. (2008), Why are climate models reproducing the observed global surface
507 warming so well?, *Geophysical Research Letters*, *35*, L18704.

508 Kuhlbrodt, T. and J. M. Gregory (2012), Ocean heat uptake and its consequences for the
509 magnitude of sea level rise and climate change, *Geophys. Res. Lett.*,
510 doi:10.1029/2012GL052952, in press.

511 Lohmann, U., L. Rotstayn, T. Storelvmo, A. Jones, S. Menon, J. Quaas, A. M. L. Ekman,
512 D. Koch, and R. Ruedy (2010), Total aerosol effect: radiative forcing or radiative flux
513 perturbation?, *Atmospheric Chemistry and Physics*, *10*(7), 3235-3246.

514 Moss, R. H., J. A. Edmonds, K. A. Hibbard, M. R. Manning, S. K. Rose, D. P. van
515 Vuuren, T. R. Carter, S. Emori, M. Kainuma, T. Kram, G. A. Meehl, J. F. B. Mitchell, N.

516 Nakicenovic, K. Riahi, S. J. Smith, R. J. Stouffer, A. M. Thomson, J. P. Weyant, and T. J.
517 Wilbanks (2010), The next generation of scenarios for climate change research and
518 assessment, *Nature*, *463*, 747-756.

519 Meinshausen, M., S. J. Smith, K. Calvin, J. S. Daniel, M. L. T. Kainuma, J-F. Lamarque,
520 K. Matsumoto, S. A. Montzka, S. C. B. Raper, K. Riahi, A. Thomson, G. J. M. Velders,
521 and D.P. P. van Vuuren (2011), The RCP greenhouse gas concentrations and their
522 extensions from 1765 to 2300, *Climatic Change*, *109*(1-2), 213-241.

523 Ramaswamy, V., O. Boucher, J. Haigh, D. Hauglustaine, J. Haywood, G. Myhre, T.
524 Nakajima, G. Y. Shi, and S. Solomon (2001), Radiative Forcing of Climate Change, in
525 *Climate Change 2001: The Scientific Basis. Contribution of Working Group I to the Third*
526 *Assessment Report of the Intergovernmental Panel on Climate Change*, edited, Cambridge
527 University Press, Cambridge, United Kingdom and New York, NY, USA.

528 Rotstayn, L. D., and J. E. Penner (2001), Indirect aerosol forcing, quasi forcing, and
529 climate response, Journal of Climate, 14(13), 2960-2975.

530 Shine, K., and P. Forster (1999), The effect of human activity on radiative forcing of
531 climate change: a review of recent developments, *Global and Planetary Change*, 205-225.

532 Skeie, R., T. Berntsen, G. Myhre, K. Tanaka, M. Kvalevag, and C. Hoyle (2011),
533 Anthropogenic radiative forcing time series from pre-industrial times until 2010,
534 *Atmospheric Chemistry and Physics*, *11*(22), 11827-11857.

535 Soden, B. J., I. M. Held, R. Colman, K. M. Shell, J. T. Kiehl, and C. A. Shields (2008),
536 Quantifying climate feedbacks using radiative kernels, *Journal of Climate*, *21*(14), 3504-
537 3520.

538 Webb, M., C. Senior, S. Bony, and J. J. Morcrette (2001), Combining ERBE and ISCCP
539 data to assess clouds in the Hadley Centre, ECMWF and LMD atmospheric climate
540 models, *Climate Dynamics*, *17*, 905–922.

541 Wyant, M., C. Bretherton, P. Blossey, and M. Khairoutdinov (2012), Fast cloud
542 adjustment to increasing CO_2 in a superparameterized climate model, *Journal of Advances*
543 *in Modeling Earth Systems*, *4*.

544 Zelinka, M. D., S. A. Klein, and D. L. Hartmann, 2012: Computing and Partitioning Cloud
545 Feedbacks Using Cloud Property Histograms. Part I: Cloud Radiative Kernels, *J. Climate*,
546 25, doi:10.1175/jcli-d-11-00248.1, 3715-3735.

547 **Table 1.** CMIP5 models employed in this paper and their feedback components computed

	Adjusted Forcing	Climate Sensitivities (K)		Transient feedbacks (Wm^{-2} K^{-1})[a]		Feedbacks (α) (Wm^{-2} K^{-1})			
	2xCO2 (Wm^{-2})	ECS	TCR	ρ	κ	LW clear-sky	SW clear-sky	Cloud:CRE -derived	Net
ACCESS1-0	2.98	3.83	2.00	1.49	0.71	1.63	-0.77	-0.08	0.78
bcc-csm1-1	3.23	2.82	1.70	1.90	0.76	1.91	-0.83	0.07	1.14
bcc-csm1-1-m	3.55	2.87	2.10	1.69	0.45	1.98	-0.68	-0.06	1.24
CanESM2	3.84	3.69	2.40	1.60	0.56	1.88	-0.71	-0.13	1.04
CCSM4	3.57	2.89	1.80	1.98	0.75	1.95	-0.87	0.16	1.23
CNRM-CM5	3.72	3.25	2.10	1.77	0.63	1.73	-0.78	0.20	1.14
CSIRO-Mk3-6-0	2.59	4.08	1.80	1.44	0.81	1.70	-0.84	-0.23	0.63
FGOALS-s2	3.85	4.17	2.40	1.60	0.68	1.46	-1.02	0.48	0.92
GFDL-CM3	2.99	3.97	2.00	1.50	0.75	1.94	-0.70	-0.48	0.75
GFDL-ESM2G	3.09	2.39	1.10	2.81	1.52	1.65	-0.61	0.26	1.29
GFDL-ESM2M	3.36	2.44	1.30	2.58	1.20	1.63	-0.58	0.33	1.38
GISS-E2-H	3.81	2.31	1.70	2.24	0.59	1.67	-0.49	0.47	1.65
GISS-E2-R	3.78	2.11	1.50	2.52	0.73	1.66	-0.36	0.48	1.79
HadGEM2-ES	2.93	4.59	2.50	1.17	0.53	1.66	-0.65	-0.37	0.64
inmcm4	2.98	2.08	1.30	2.29	0.86	1.98	-0.67	0.12	1.43
IPSL-CM5A-LR	3.10	4.13	2.00	1.55	0.80	1.99	-0.53	-0.70	0.75
IPSL-CM5B-LR	2.66	2.61	1.50	1.77	0.75	1.88	-0.59	-0.28	1.02
MIROC5	4.13	2.72	1.50	2.75	1.23	1.85	-0.84	0.51	1.52
MIROC-ESM	4.26	4.67	2.20	1.93	1.02	1.93	-0.83	-0.19	0.91
MPI-ESM-LR	4.09	3.63	2.00	2.05	0.92	1.79	-0.71	0.04	1.13
MPI-ESM-P	4.31	3.45	2.00	2.16	0.91	1.80	-0.65	0.10	1.25
MRI-CGCM3	3.25	2.60	1.60	2.03	0.78	1.99	-0.83	0.09	1.25
NorESM1-M	3.11	2.80	1.40	2.22	1.11	1.86	-0.86	0.11	1.11
Multi model mean	**3.44**	**3.22**	**1.82**	**1.96**	**0.83**	**1.81**	**-0.71**	**0.04**	**1.13**
90% uncertainty	0.84	1.32	0.63	0.73	0.41	0.25	0.24	0.53	0.51

548

549 [a]1% CO_2 increase scenario per year numbers are used to derive TCR, ρ and κ. 4xCO_2
550 abrupt CO_2 scenario changes are used to determine the other quantities. Method follows
551 *Andrews et al. [2012b]* updating to account for additional model availability. Larger
552 feedback values represent greater radiative damping of surface temperature anomalies and
553 therefore smaller equilibrium climate sensitivity.

554 **Table 2.** AFs for different scenarios given at 2003 (2001-2005 average), 2010 (2008-
555 2012 average) and 2095 (2091 to 2099)

	Adjusted forcing (Wm^{-2}) for scenario and period								
	Hist 2003	HistGHG 2003	HistNat 2003	Hist NonGHG 2003	RCP 4.5 2010	RCP2.6 2095	RCP4.5 2095	RCP6.0 2095	RCP8.5 2095
ACCESS1-0	1.1				1.4		3.3		6.2
bcc-csm1-1	2.2	2.0	0.1	0.0	2.0	2.5	3.3	4.5	7.0
bcc-csm1-1-m	2.2				2.2	1.9	3.3	4.3	7.0
CanESM2	2.0	2.4	0.1	-0.5	2.2	2.9	4.3		8.4
CCSM4	2.5	2.3	0.1	0.1	2.7	2.8	4.3	5.4	8.3
CNRM-CM5	1.5	2.2	0.1	-0.8	1.2	2.3	3.7		6.9
CSIRO-Mk3-6-0	0.9	1.4	0.1	-0.6	1.0	1.9	2.8	3.4	5.7
FGOALS-s2	2.3				2.8	2.5	4.3	6.5	10.0
GFDL-CM3	1.1	2.9	0.5	-2.2	1.7	3.1	4.2	4.9	7.2
GFDL-ESM2G	2.0				1.9	1.2	2.8	3.9	6.4
GFDL-ESM2M	2.0	2.5	0.2	-0.7	2.2	2.5	3.5	4.9	7.3
GISS-E2-H	2.3	3.2	0.2	-1.0					
GISS-E2-R	2.5	3.3	0.2	-0.9	2.5	2.6	4.7	5.9	8.6
HadGEM2-ES	0.8	1.9	0.1	-1.1	1.0	1.7	2.9	4.0	5.9
inmcm4	1.7				1.9		3.8		7.3
IPSL-CM5A-LR	1.9	2.4	0.2	-0.7	1.8	2.2	3.5	4.3	7.1
IPSL-CM5B-LR	1.0								
MIROC5	1.6				2.0	3.0	4.5	5.3	8.7
MIROC-ESM	1.1	2.2	0.0	-1.0	1.5	2.8	4.0	5.1	8.2
MPI-ESM-LR	2.1				2.3	2.2	3.9		7.7
MPI-ESM-P	2.3								
MRI-CGCM3	1.2	2.1	0.2	-1.1	1.2	2.1	3.6	4.3	7.0
NorESM1-M	**1.4**	**2.3**	**0.0**	**-0.9**	**1.7**	**2.0**	**3.6**	**4.2**	**7.0**
Multi model mean	**1.7**	**2.4**	**0.1**	**-0.8**	**1.9**	**2.3**	**3.7**	**4.7**	**7.4**
90% uncertainty	**0.9**	**0.8**	**0.2**	**0.9**	**0.9**	**0.8**	**0.9**	**1.3**	**1.8**

556

557 Table 3 Temperature changes since preindustrial times for different scenarios given at
558 2003 (2001-2005 average), 2010 (2008-2012 average) and 2095 (2091 to 2099)

	Temperature change since pre-industrial (K) for scenario and period								
	Hist 2003	Hist GHG 2003	Hist Nat 2003	Hist NonGHG 2003	RCP 4.5 2010	RCP2.6 2095	RCP4.5 2095	RCP6.0 2095	RCP8.5 2095
ACCESS1-0	0.6				0.8		2.7		4.8
bcc-csm1-1	1.2	1.4	0.1	-0.3	1.4	2.0	2.5	3.1	4.6
bcc-csm1-1-m	1.7				1.8	2.0	2.7	3.2	4.8
CanESM2	1.0	1.6	-0.1	-0.4	1.2	2.3	3.2		5.5
CCSM4	1.3	1.3	0.0	-0.1	1.3	1.9	2.7	3.2	4.7
CNRM-CM5	1.0	1.3	0.1	-0.4	1.1	1.8	2.7		4.5
CSIRO-Mk3-6-0	0.7	1.2	0.2	-0.7	0.7	1.9	2.5	2.9	4.8
FGOALS-s2	1.8				2.0	2.1	3.0	4.4	6.6
GFDL-CM3	0.3	1.8	-0.1	-1.4	0.9	2.1	2.9	3.5	5.1
GFDL-ESM2G	0.8				1.0	0.8	1.6	2.2	3.6
GFDL-ESM2M	0.8	1.0	0.0	-0.2	0.8	1.3	1.8	2.3	3.5
GISS-E2-H	1.2	1.4	0.1	-0.3					
GISS-E2-R	1.1	1.2	0.2	-0.3	1.1	1.4	2.2	2.6	3.7
HadGEM2-ES	0.5	1.5	0.0	-1.0	0.7	1.7	2.8	3.6	5.2
inmcm4	0.8				0.9		2.0		3.5
IPSL-CM5A-LR	1.4	1.9	0.2	-0.7	1.5	2.3	3.3	3.8	5.8
IPSL-CM5B-LR	0.9								
MIROC5	0.6				0.8	1.4	2.1	2.5	4.0
MIROC-ESM	0.7	1.3	0.0	-0.6	1.0	2.3	3.1	3.7	5.5
MPI-ESM-LR	1.0				1.2	1.5	2.5		4.6
MPI-ESM-P	1.0								
MRI-CGCM3	0.6	1.1	0.1	-0.6	0.5	1.3	2.1	2.4	3.9
NorESM1-M	0.7	1.2	-0.1	-0.4	1.0	1.4	2.2	2.5	4.0
Multi model mean	**1.0**	**1.4**	**0.1**	**-0.5**	**1.1**	**1.8**	**2.5**	**3.1**	**4.6**
90% uncertanity	**0.6**	**0.4**	**0.2**	**0.6**	**0.6**	**0.7**	**0.8**	**1.1**	**1.4**

559

560

561

562 **Table 4.** AFs calculated for aerosol-only perturbations in fixed SST experiments
563 compared to AFs for 2003 from the FT06-updated *Historical-nonGHG* residual scenario.

Model	Net	Clear-sky	Cloud: CRE derived
	Forcing (Wm^{-2})		
	Fixed SST		
CanESM2	-0.86	-0.59	-0.28
CSIRO-Mk3	-1.41	-1.04	-0.37
HadGEM2-ES	-1.23	-0.35	-0.88
	FT06-updated residual		
CanESM2	-0.51	-0.33	-0.18
CSIRO-Mk3	-0.61	-0.59	-0.02
HadGEM2-ES	-1.12	-0.66	-0.46

564

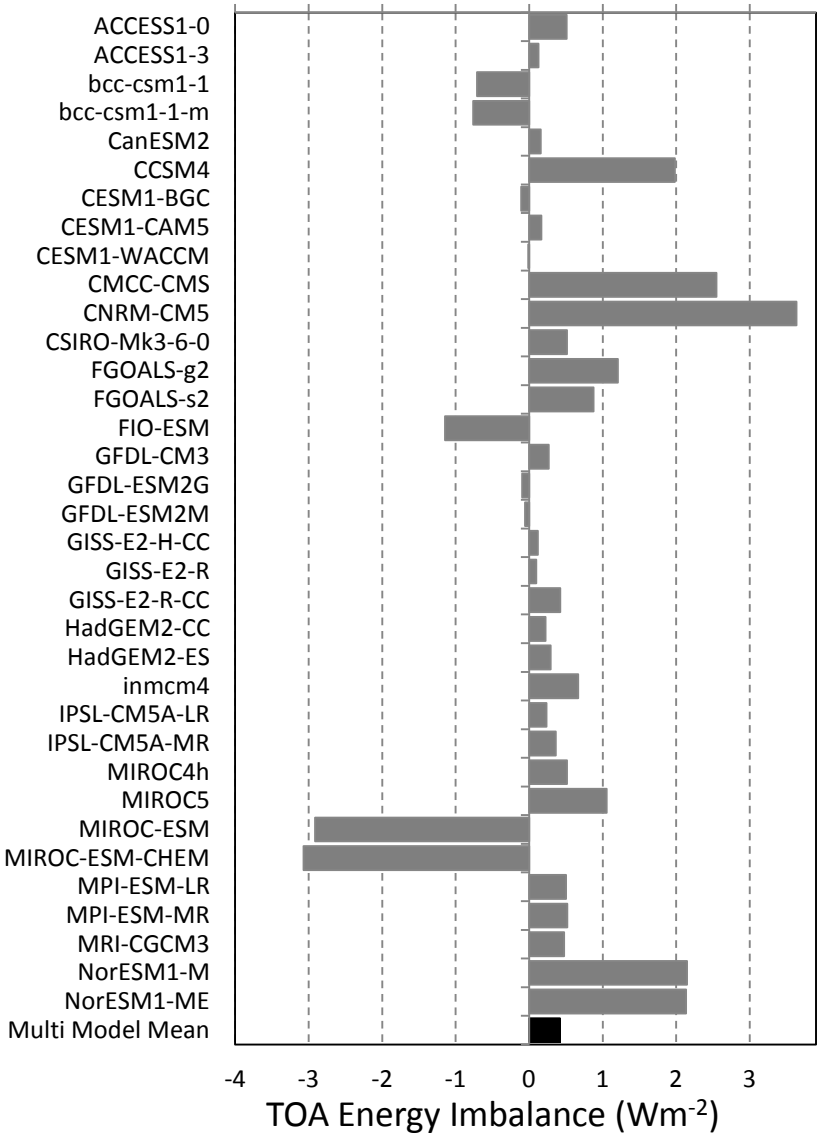

565

566 **Figure 1.** Preindustrial TOA energy imbalance (Wm^{-2}) for the CMIP5 models. These were
567 averaged over the entire preindustrial control period. Note additional models are included,
568 compared to the main analysis (compare Table 1).

569

570

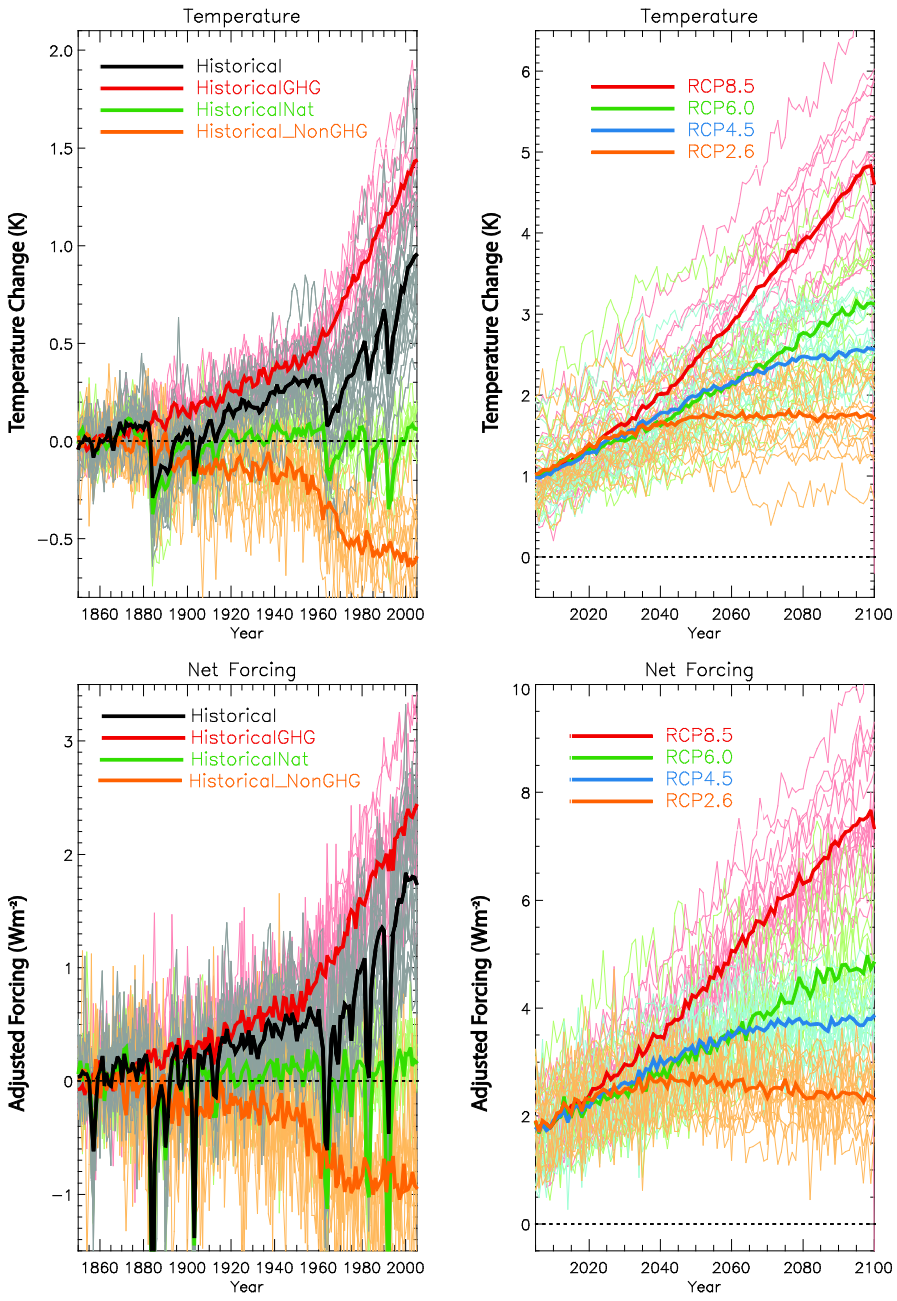

571

572 **Figure 2.** The globally averaged surface temperature change since preindustrial times
573 (top) and computed net AF (bottom). Thin lines are individual model results averaged
574 over their available ensemble members and thick lines represent the multi-model mean.
575 The *Historical-nonGHG* scenario is computed as a residual and approximates the role of
576 aerosols (see Section 2).

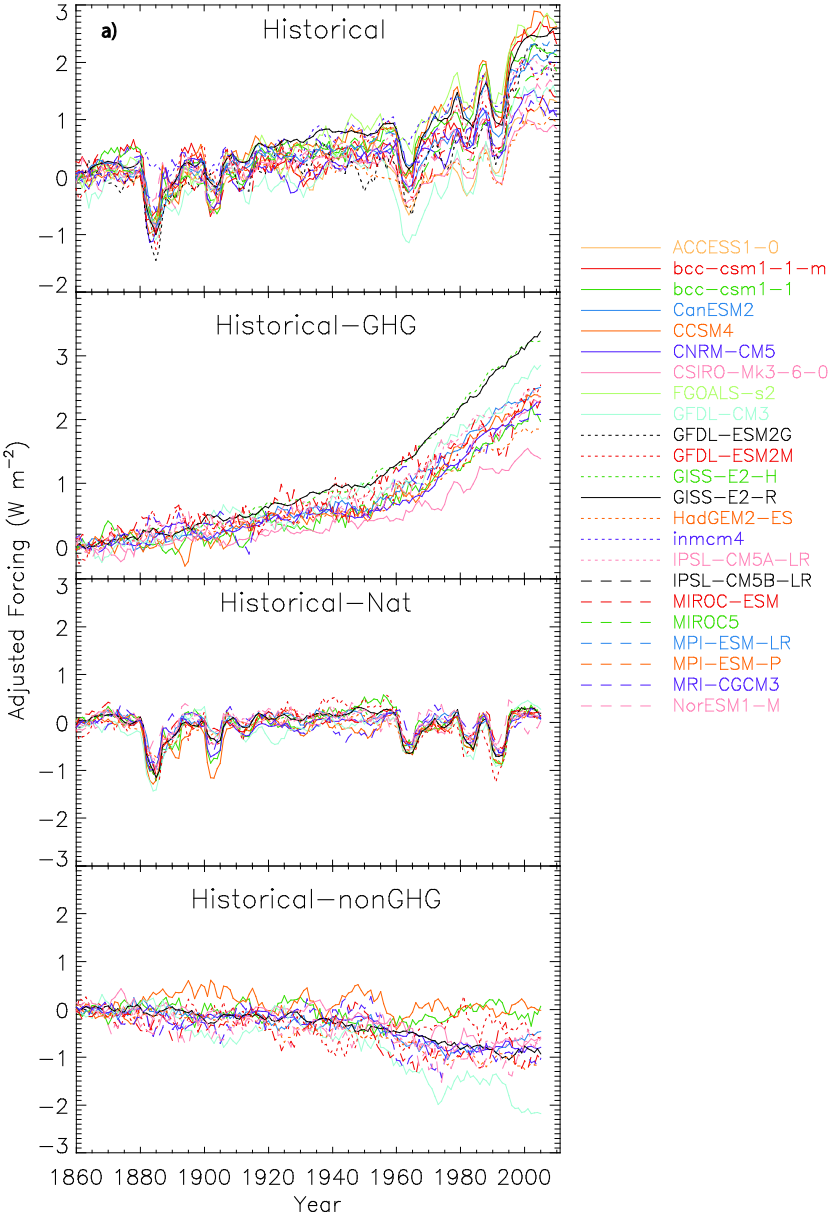
a)
Historical
Historical−GHG
Historical−Nat
Historical−nonGHG
Adjusted Forcing (W m−2)
Year
1860 1880 1900 1920 1940 1960 1980 2000
ACCESS1−0
bcc−csm1−1−m
bcc−csm1−1
CanESM2
CCSM4
CNRM−CM5
CSIRO−Mk3−6−0
FGOALS−s2
GFDL−CM3
GFDL−ESM2G
GFDL−ESM2M
GISS−E2−H
GISS−E2−R
HadGEM2−ES
inmcm4
IPSL−CM5A−LR
IPSL−CM5B−LR
MIROC−ESM
MIROC5
MPI−ESM−LR
MPI−ESM−P
MRI−CGCM3
NorESM1−M

577

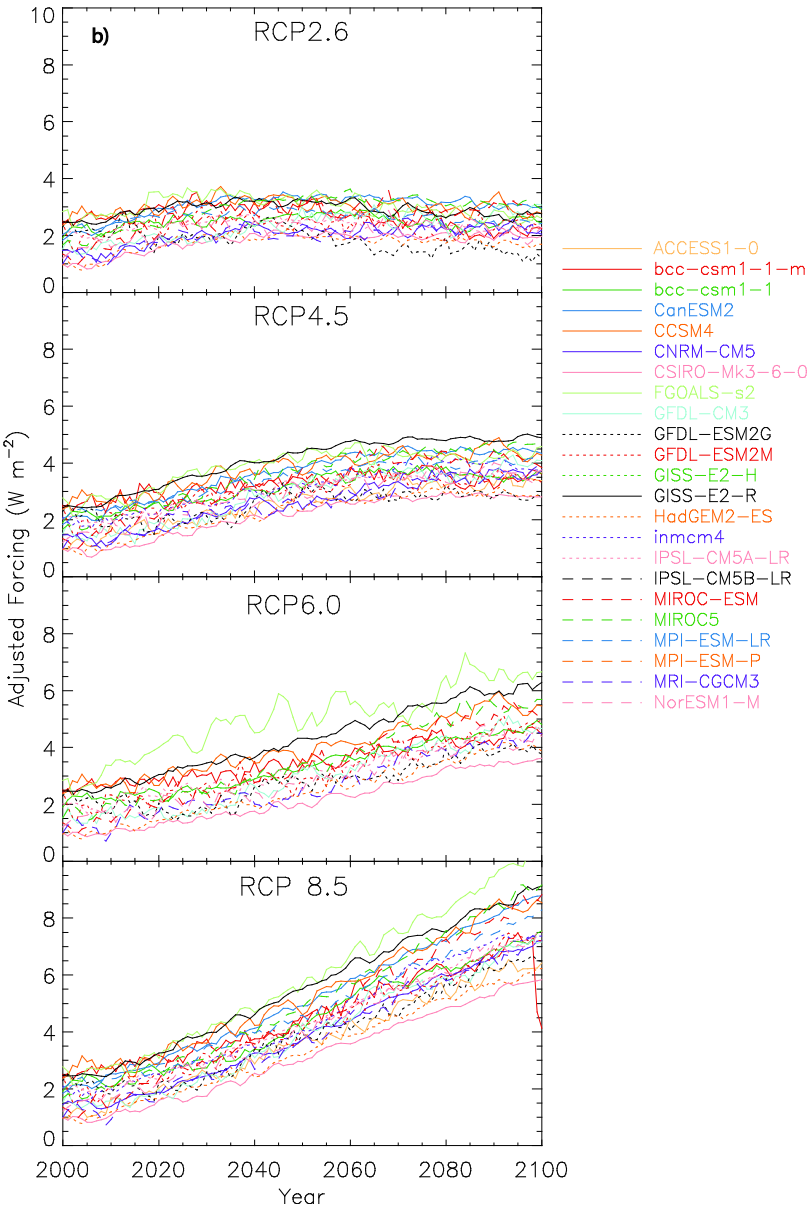

578

579 **Figure 3.** Time series of AF from the different a) historical scenarios and b) future

580 scenarios.

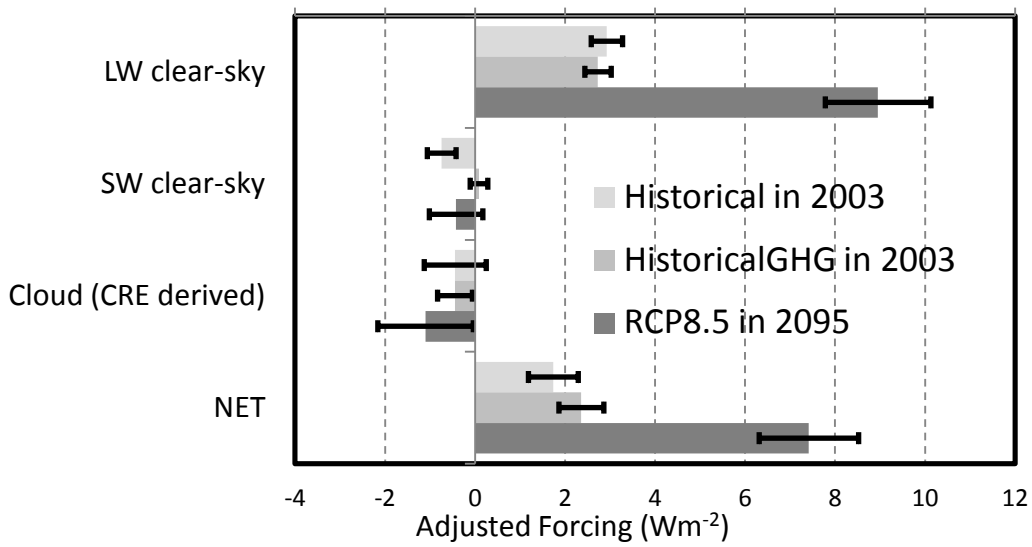

581

582 **Figure 4.** Diagnosed AFs (since preindustrial) for the *Historical*, *HistoricalGHG*, and
583 *RCP8.5* scenarios. The historical scenarios give the AF for 2003 (2001-2005 average) and
584 the RCP scenario for 2095 (2091-2099 average). AFs are given for the LW clear-sky
585 forcing, the SW clear-sky forcing, the CRE-derived cloud forcing, and the net forcing.
586 Note that the CRE-derived cloud forcing includes a component due to cloud masking
587 effects. Error bars represent the standard deviation of the model range.

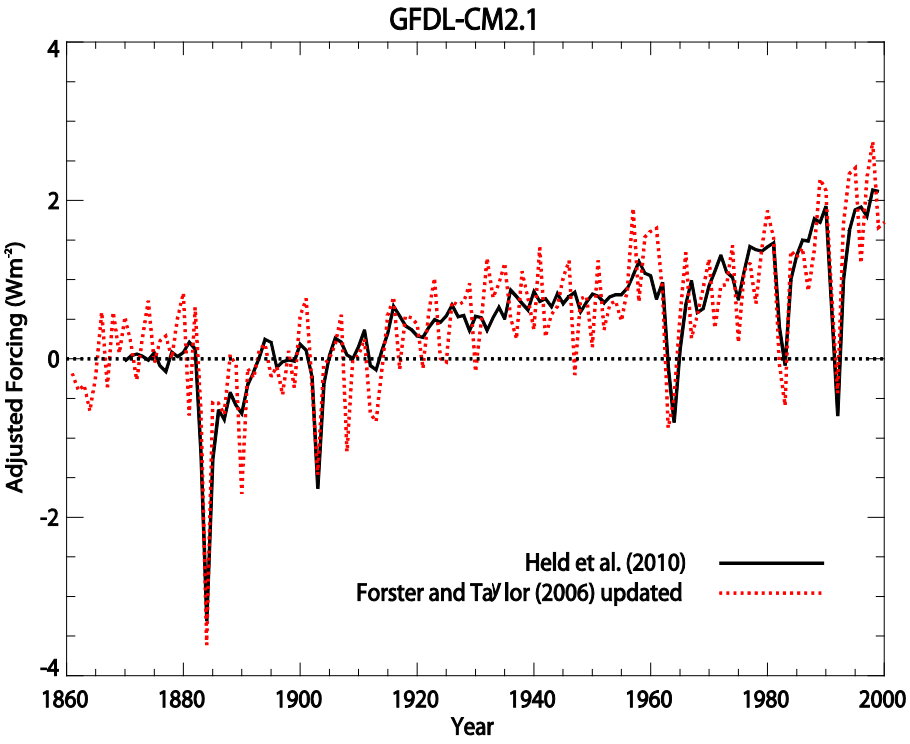

588

589 **Figure 5.** A comparison of two methods of calculating AF in the CMIP3 GFDL CM2.1
590 model. The black line is a calculation of AF that uses two prescribed SST integration
591 experiments, with and without forcing agents, and compares TOA fluxes [*Held et al.*,
592 2010]. The AF in the red line employs our FT06-updated method in the same model.

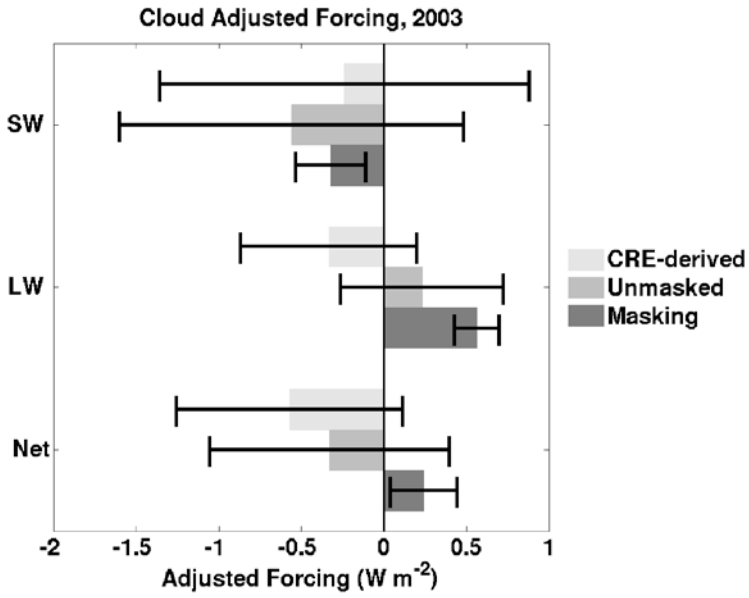

593

594 **Figure 6.** Multi-model mean and standard deviation of the global mean Cloud AFs for the
595 unmasked (i.e., cloud kernel-derived) AF and CRE-derived AF. Cloud AFs are given for
596 LW, SW, and net variables for five GCMs averaged over years 2001-2005 of the
597 *Historical* simulations. Unmasked minus CRE-derived cloud AFs gives an estimate of the
598 cloud masking of the forcing.

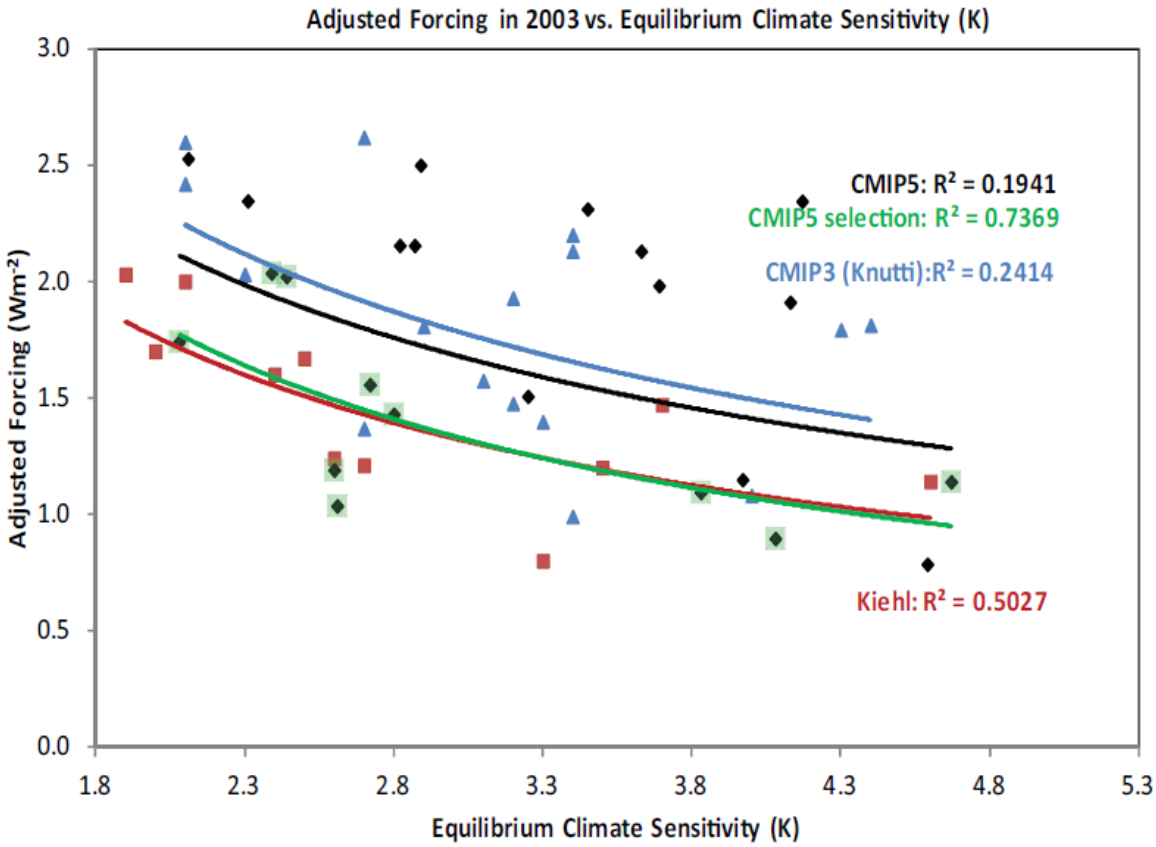

599

600 **Figure 7.** The relationship between 2003 AF and ECS in CMIP5 and earlier generations
601 of models. CMIP3 numbers are taken from *Knutti [2008]* and older models from *Kiehl*
602 *[2007]*. The solid line fits are made using the inverse relationship between forcing and
603 climate sensitivity postulated by *Kiehl* [*2007*]. Data is shown for all CMIP5 models as
604 black diamonds, using the *Historical* simulation. A subset of CMIP5 models is shown by
605 the green squares that are within the 90% uncertainty range of the observed 100 year
606 linear temperature trend. These models have 1906-2005 linear trends between 0.56 K and
607 0.92 K, the *IPCC [2007]* 90% uncertainty range. R^2 values are computed with respect to
608 the non-linear fit shown.

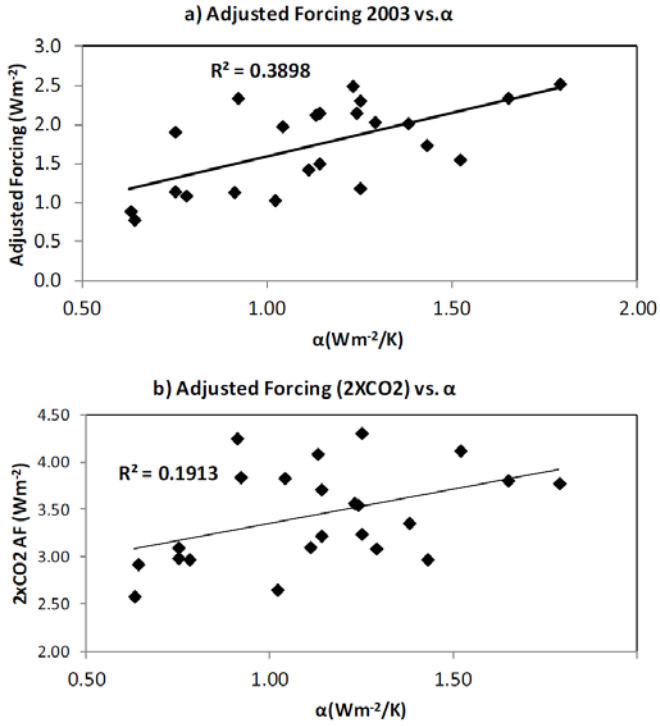

609

610 Figure 8. Scatterplots of *Historical* 2003 AF against α (a) and 2xCO_2 AF against α (b).

611

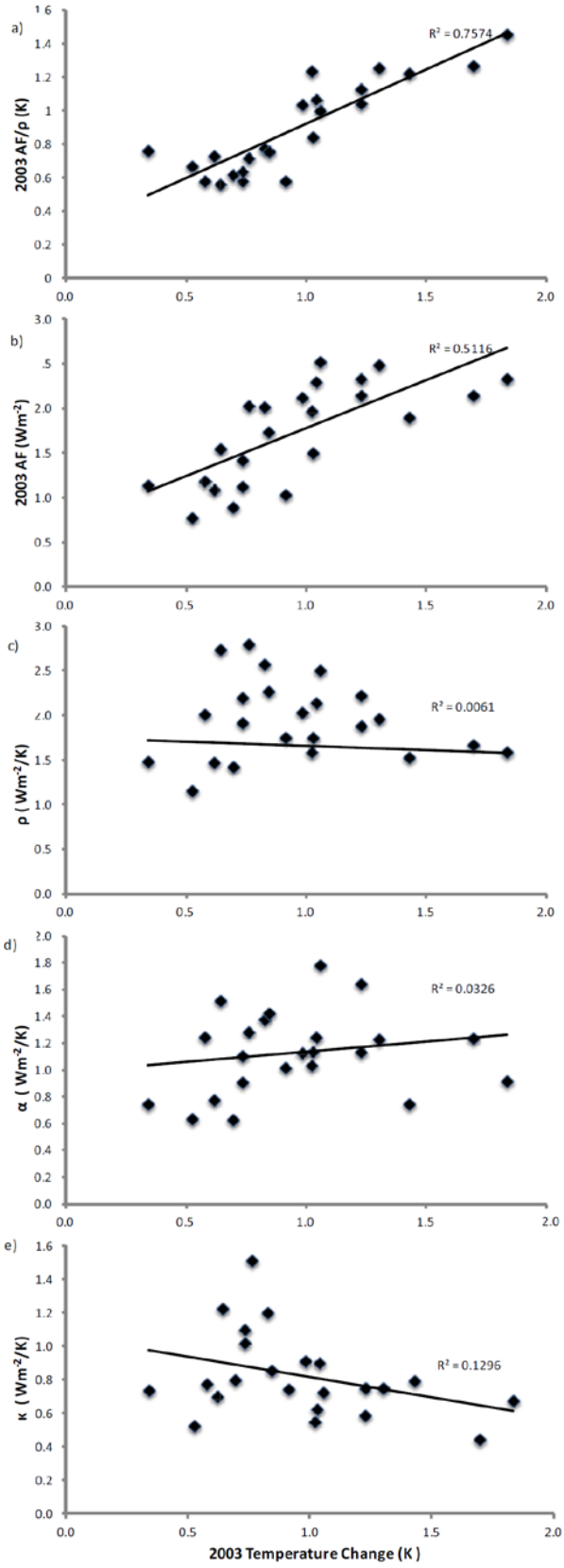

Figure 9. Scatterplots of a) AF/ρ, b) AF, c) ρ, d) α, and e) κ against the temperature change in 2003 from the *Historical* simulation.

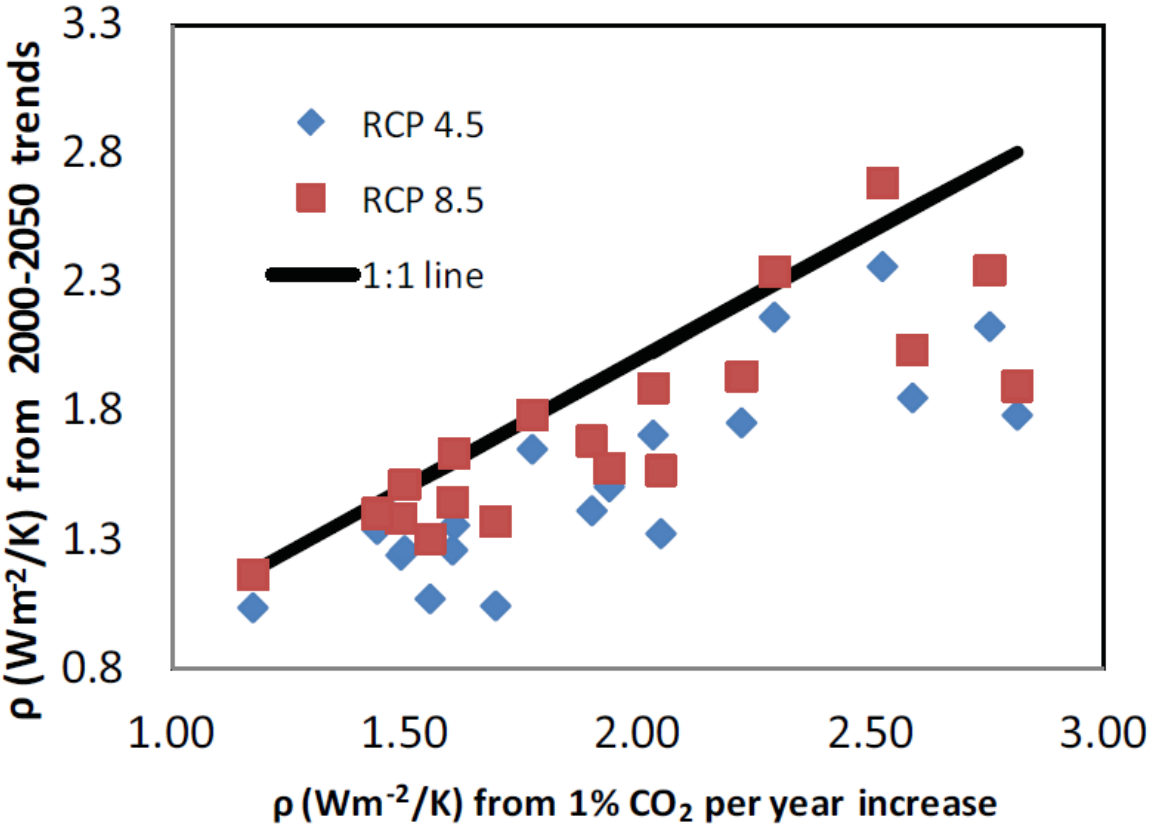

617

618 **Figure 10.** Resistance (ρ) derived from 2000-2050 trends in the *RCP 4.5* and *RCP 8.5*
619 scenarios compared to those derived for the 1% per year CO_2 increase scenario that is used
620 to diagnose the TCR. The black line represents the 1:1 relationship.

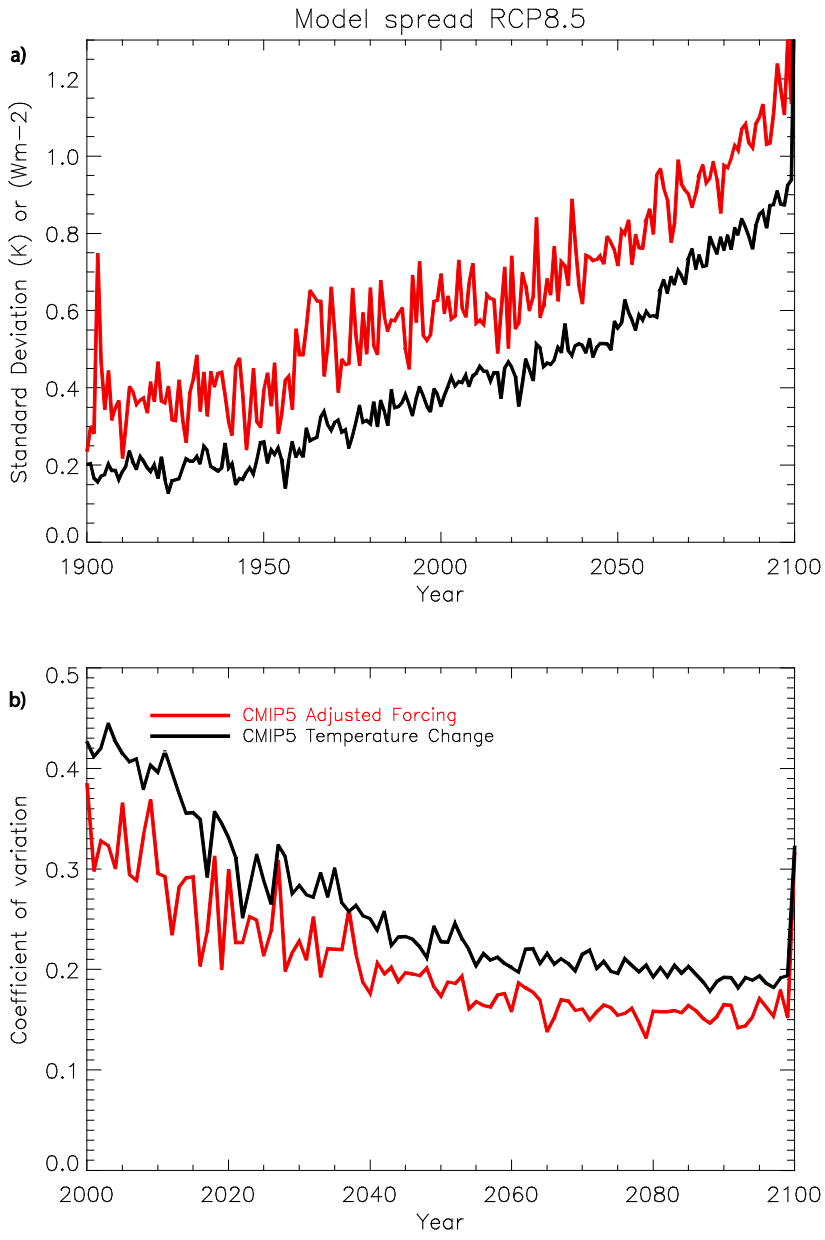

621

622 **Figure 11.** The a) standard deviation and b) coefficient of variation (standard
623 deviation/mean) between models for temperature (black) and AF (red) as a function of
624 time for the *RCP8.5* scenario. Note the different time scales on the x axis.

625

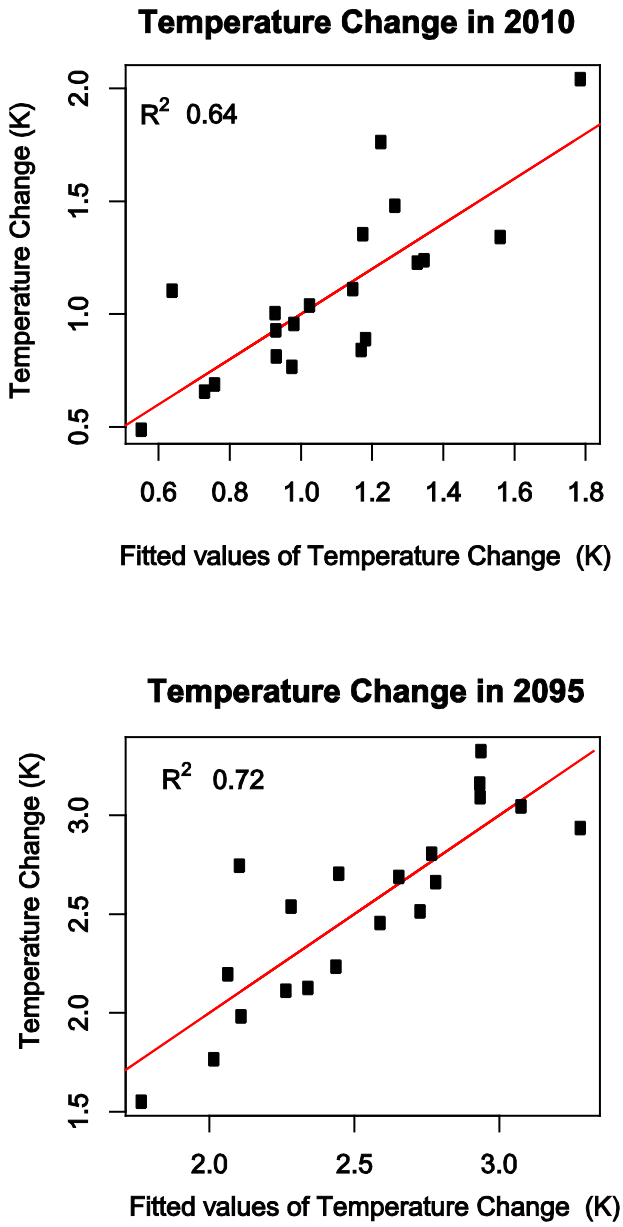

626

627 **Figure 12.** Modeled temperature changes for 2010 and 2095 for the *RCP 4.5* scenario,
628 compared to fitted values from the linear regression. The red line represents the 1:1
629 relationship. The fitted values are for the linear regression with both α and AF included as
630 explanatory variables.

631